Rician Noise Level Estimation and Constraint Model for MRI Restoration

Juncheng Guo, Jia Liu

***Abstract*—We propose a new Rician noise level estimation method to use for MRI restoration in this paper. This method relies on the application of a novel distance as the primary constraint, combined with the total variation as a prior condition. Based on the estimated noise level, we present a non-parametric constraint model, which minimizes the regularization term while maintaining constraints on the fidelity term. This model can be successfully solved using the primal-dual algorithm. Experimental results demonstrate the effectiveness and efficiency of the proposed method in estimating Rician noise.**

***Index Terms*—MRI; Image Restoration; Rician Noise Estimation; Total Variation**

I. Introduction

THE magnetic resonance imaging (MRI) technique is utilized to generate comprehensive images of the human internal body, offering unparalleled detailed insights that render it an indispensable tool for diagnosing potentially fatal diseases. Utilizing the data obtained from the sensors, the system reconstructs sectional images and enables the generation of three-dimensional images at any desired angle. The acquired raw data in MRI are formally complex values represented in a frequency domain (k-space). Both the real and imaginary components of these data are affected by zero-mean, uncorrelated Gaussian noise, with equal variances for both components. While the complex data inherently encompass all pertinent information, After estimating the signal amplitude, it is customary to convert the data into magnitude images, as these are more intimately connected to physiological and anatomical characteristics. [22], [26], [15], [16]. Then, the data's distribution undergoes a transformation from Gaussian to Rician [18]. However, in areas of low image intensity, the Rician distribution converges towards the Rayleigh distribution, whereas in high-intensity areas, it deviates from the Gaussian distribution. The mean value of Rician noise fluctuates according to the local image intensity, making it distinct from additive Gaussian noise, which remains unaffected by the signal [17]. Therefore, the complexity of the MRI image restoration problem persists owing to the diverse distributions it encompasses.

There are a variety of study methods for MRI denoising problems, such as approaching the problem of MRI filtering with standard denoising algorithms designed for homoskedastic observations [11]. Furthermore, numerous applications utilizing statistical analysis methodologies, including functional MRI and voxel-based morphometry, often derive their conclusions from underlying assumptions related to noise characteristics [16], [19]. During the image formation process, the presence of various noise sources leads to additive Gaussian noise. However, magnitude magnetic resonance (MR) images often encounter Rician noise. These images, inherently composed of data acquired by a quadrature detector, are essentially two- or three-dimensional arrays made up of complex numbers [14]. Typically, they can be viewed as a pair of images representing the real and imaginary parts of a complex array. Therefore, several artifacts and noise sources typically affect MR images. When using MRI, the raw data, which hold complex values, are acquired in the spatial frequency domain and are corrupted by Gaussian-distributed noise.

In most image processing problems, the data are often considered corrupted by noise, so estimating the noise level is an important factor in obtaining good results. For example, in the classic ROF model,

$$\min_u TV(u) + \lambda \|u - f\|_2^2,$$

where f is viewed as an image with additive white Gaussian noise, and λ is a parameter determined by noise level. Without a known λ (which means the noise level is unknown), the ROF model cannot be used to obtain a result. In many methods of image processing, the noise level is treated as known data and related parameters have been well tuned for the noise level. However, in the real world, noise level is always unknown, and estimating noise level becomes an important task.

In most common situations, the noise can be regarded as additive white Gaussian noise, and the noise level is characterized by its standard deviation. Some filter-based methods have been proposed [2], [20], [13]. These algorithms mainly use a filter to prevent subtle textures from getting an approximation of a clean image and treat the differences between the filtered image or the original data as the noisy information. Wavelet-based methods use wavelet transforms and view the high-frequency parts as noise [24]. Patch-based methods try to find areas where the clean image is smooth or constant[12], [21]. Subsequently, they estimate the noise level by calculating the standard deviation within these identified areas.

During the MRI data calculation and transmission process, Rician noise arises when both the real and imaginary parts are corrupted by two additive white Gaussian noises, each having the same standard deviation, denoted as σ. Background-based methods are proposed since Rician noise obeys a Rayleigh distribution when the true value is zero [23]. Wavelet-based methods try to find the estimator of

Manuscript received Jan 25, 2024; revised Jan 1, 2025.

This work was supported by the Scientific and Technological Research Projects in Henan Province (242102210146); the Key Scientific Research Projects in Universities in Henan Province (24B110006); the Research Project of Henan Polytechnic (2024J046).

Juncheng Guo is an associate professor of the Basic Education Department, Henan Polytechnic, Zhengzhou, 450046, China (Corresponding author, email: acheng2090@126.com).

Jia Liu is an associate professor of Zhengzhou University of Economics and Business, Zhengzhou, 451191, China (email: lyoujya@foxmail.com).

Rician noise by the relationship between Gaussian noise and σ [9].

Based on the MAP method [5], the MRI restoration models utilize the probability density function used in Rician noise. It necessarily requires not only the noise level need be known but also a parameter should be tuned.

Thus, we assume that the image is large enough and that most of its area is smooth, a novel method is proposed to estimate the Rician noise level using patches and histograms. The main contributions are summarized as follows.

- Using the high resolution of MRI, the pixel values in the noiseless image can be approximately seen as constant in most of the patches. That is to say, by presuming that the variations in pixel values within each patch represent noise, it is possible to estimate the noise level. This means that most of the estimated values will be around the real noise level.
- We produce a novel distance functions as a constraint condition, and the total variation is used as a priori condition. The advantage of this model is that the noise level is directly used and there are no parameters, which can circumvent the parameter training problems commonly encountered in typical image processing.
- The formulated model constitutes a non-smooth optimization problem, thus rendering the primal-dual method a suitable approach for solving it. The mathematical properties of the algorithm are analyzed, and some numerical implementations show that the good results can be achieved.

The arrangement of the paper is as follows. Some basic information about Rician noise and the image restoration model is reviewed in section 2. The method for Rician noise level estimation is proposed in section 3. A constraint model for MRI restoration and the algorithm for solving the model is in section 4. Some number experiments are shown in section 5, and section 6 is the conclusion.

II. Rician noise

In the imaging system, the modeling of noise in MRI varies based on the number of coils. In a single-coil setup, the noise distribution in MRI can be characterized by a Rician distribution, assuming that the real and imaginary components of the MRI signal follow uncorrelated Gaussian distributions with zero mean and equal variance [4]. Conversely, in a multicoil system (parallel MRI), the noise magnitude conforms to a non-central Chi distribution when employing a sum-of-squares (SoS) reconstruction technique [8]. Similarly, noise within MRI images obtained through the process of generalized auto-calibrating partially parallel acquisition (GRAPPA) reconstruction can also be described by a non-central Chi distribution [6]. Essentially, the Rician distribution represents a specific instance of the non-central Chi distribution.

In MRI reconstruction, due to the use of a complex Fourier transform, the Gaussian noise is added to both the real and imaginary images, and the corrupted data are the absolute values of the complex images.

$$f = \sqrt{(u+n_1)^2 + n_2^2}, \tag{1}$$

where f is the noisy image, and u is original image, $n_1, n_2 \sim \mathcal{N}(0,\sigma)$, and n_1, n_2 are independent.

So the image is corrupted by Rician noise, and its probability density function is

$$p\left(f|u\right) = \frac{f}{\sigma^2} e^{-\frac{u^2+f^2}{2\sigma^2}} I_0\left(\frac{uf}{\sigma^2}\right). \tag{2}$$

In the above formula, I_0 is the modified Bessel function of the first kind with order zero. The definition of the modified Bessel function of the first kind with order n is

$$I_n(x) = \frac{1}{\pi}\int_0^\pi \cos(n\theta)\exp(x\cos\theta)d\theta. \tag{3}$$

Thus, the Rician noise is neither additive nor independent and induces a bias in the noisy image. However, if the noise level σ is relatively low compared with the signal value, Rician noise has little difference from Gaussian noise. To model this noise, MAP method is tried by solving

$$\max_u P(u|f),$$

with Bayes's rules, which known as

$$P(u|f) = \frac{P(f|u)P(u)}{P(f)}.$$

We can rewrite it as

$$\begin{aligned}
\max_u P(u|f) &= \max_u \frac{P(f|u)P(u)}{P(f)} \\
&= \min_u -\log\left(P(f|u)\right) - \log(P(u)) \\
&= \min_u -\int_\Omega \log\left(P\left(f(x)|u(x)\right)\right)dx - \log(P(u)) \\
&= \min_u \int_\Omega \frac{u^2}{2\sigma^2}dx - \int_\Omega \log\left(I_0\left(\frac{uf}{\sigma^2}\right)\right)dx \\
&\quad - \log\left(P(u)\right).
\end{aligned}$$

The term "$-\log(P(u))$" can be viewed as a regularization term like the total variation $\lambda\int_\Omega |Du|dx$, and the MAP model is

$$\min_u \int_\Omega \frac{u^2}{2\sigma^2}dx - \int_\Omega \log\left(I_0\left(\frac{uf}{\sigma^2}\right)\right)dx + \lambda\int_\Omega |Du|dx.$$

In this model, we can see that we not only need to know a noise level σ but also a tuned parameter λ.

III. Noise level estimation

In many image restoration models, the noise level is always treated as already known and the weight parameter λ is tuned to achieve the best solution for certain σ. But in many situations, the relation between λ and σ is not quite clear. Therefore, a lot of experiments are needed to reset λ for a different σ. However, in real schemes, σ is an unknown variable, meaning that a good λ cannot be estimated. We are sure that it is important to estimate the noise level.

The difficulty of noise level estimation is mainly how to distinguish the noise from the detail texture of the original image. In natural images, image data often contain more smooth areas. That is to say, the gradient matrix of the image information is generally sparse. We know that the ℓ^1 norm tends to sparsen the data, which is why the total variation regularization term could be a good regularization term in image processing. Based on this feature, we use a patch-based method here. Specifically, we estimate the noise level

in each patch by assuming that the original image remains constant across all patches. This assumption holds true for the majority of patches.

As a patch-based method, we select noisy images to generate a series of patches by sliding the window pixel by pixel. In each patch, based on the definition of Rician noise(1),

$$\begin{aligned}\operatorname{var}\left(f^2\right) =& E\left(f^2-E(f^2)\right)^2\\ =& E[u^2-E\left(u^2\right)+n_1^2-E\left(n_1^2\right)+n_2^2-E\left(n_2^2\right)+\\ & 2un_1-2E\left(un_1\right)]^2\\ =& E\left(a+b+c+d\right)^2,\end{aligned}$$

here, $a=u^2-E(u^2)$, $b=n_1^2-E(n_1^2)$, $c=n_2^2-E(n_2^2)$, $d=2un_1-2E(un_1)$. In the case of separate calculations, each expanded term can be described as

$$\begin{cases} E\left(a^2\right)=\operatorname{var}\left(u^2\right)\\ E\left(b^2\right)=\operatorname{var}\left(n_1^2\right)=2\sigma^4\\ E\left(c^2\right)=\operatorname{var}\left(n_2^2\right)=2\sigma^4\\ E\left(d^2\right)=4E\left(u^2n_1^2\right)-4[E\left(un_1\right)]^2=4\sigma^2E\left(u^2\right)\\ E\left(ab\right)=E(ac)=E(ad)=0\\ E(bc)=E(bd)=E(cd)=0.\end{cases}$$

Therefore, we can get

$$\operatorname{var}\left(f^2\right)=\operatorname{var}\left(u^2\right)+4\sigma^4+4\sigma^2E\left(u^2\right).$$

Based on the definition of Rician noise $E\left(f^2\right)=E\left(u^2\right)+2\sigma^2$, rewrite the above formula as $\operatorname{var}\left(f^2\right)=\operatorname{var}\left(u^2\right)+4\sigma^2E\left(f^2\right)-4\sigma^4$. Reverse the calculation of σ, and we can get the estimation of noise intensity

$$\sigma=\frac{1}{2}\sqrt{E\left(f^2\right)-\sqrt{2E\left(f^2\right)^2-E\left(f^4\right)+\operatorname{var}\left(u^2\right)}}, \quad (4)$$

where f is the noisy image, $E(\cdot)$ is expectation value, u is original image, and $var(\cdot)$ is variance.

Since the value of u is unknown, we can assume it to be constant in each patch. Therefore, we can conclude that $\operatorname{var}\left(u^2\right)=0$. Using this approach, we can obtain a sequence of σ, noted $\{\sigma_i|i=1,2,\ldots,N\}$, where N is the number of patches. Then, the histograms of $\{\sigma_i|i=1,2,\ldots,N\}$ can be made, and the σ_i corresponding to the maximum value in the histogram is viewed as the noise level.

Using histograms is an efficient way to determine the distribution of $\{\sigma_i\}$, where the group distance is determined by acceptable error and the number of patches. Since we assume $u=0$ in each patch, some estimations should contain boundary information and may surpass the real noise level. These estimations can be denoted as $\{\sigma_{B,i}\}$, and others are generated in homogeneous areas, noted as $\{\sigma_{H,i}\}$, while the real noise level is σ_0. Therefore, we can get

$$E(\sigma_{H,i})=\sigma_0, \quad (5)$$

$$\sigma_{B,i}>\sigma_0. \quad (6)$$

For $\{\sigma_{H,i}\}$, on one side, if the noise is Gaussian, the top of the histogram of $\{\sigma_{H,i}\}$ should be σ_0. On the other side, Rician noise trends to get another peak at some point smaller than σ_0. To deal with this, we just turn the size of patch n large enough, because

$$n\to\infty,\sigma_{H,i}\to\sigma_0, \quad (7)$$

the larger n can ensure the maximum of histogram is around σ_0. If there is a large enough homogeneous area that does not contain boundary information, we could even get $min(\sigma_i)=\sigma_0$. For $\{\sigma_{B,i}\}$, on the one hand, the cardinal number of this set is smaller compared to N. On the other hand, since boundary information cannot be the same in many patches, $\{\sigma_{B,i}\}$ can't form a significant peak in the histogram of $\{\sigma_i\}$. From the above, the patch size n should not be small, and boundary information should be sparse. This means the original image requires the conditions as follows.

- The image is large to ensure that there are enough pixels in the homogeneous patches to reduce the effects of Rician noise.
- Compared with boundary regions, homogeneous areas are much more numerous and host most of the pixels. These conditions also mean the picture should be large and the total variation should be pretty low.

IV. Numerical method to the proposed model

In this part, we will examine the numerical technique associated with our proposed model. Prior to deducing the conjugate representation of the regularization component within the model, we offer a streamlined explanation of the total variation theory. Following this, we turn our attention to the primal-dual approach by reformulating our model into a minimization-maximization problem. Based on the estimated noise level, a constraint model without parameters is given by minimizing the regulation term while constraining the fidelity term. This proposed model can be solved successfully by the primal dual algorithm.

A. Total variation theory

Many problems in computer vision can be expressed in the form of energy minimisations. The total variation has been introduced as a regularizing criterion for solving inverse problems. Because our proposed model is closely related to the total variation function, this subsection mainly reviews some related total variation theory used in many classic image denoising works [1], [10], [25].

Since its inception in 1992, the Rudin-Osher-Fatemi (ROF) model, also referred to as total variation denoising [10], has garnered numerous applications across various fields. The total variation regularized model stands out as a potent tool for image noise removal, attributed to its ability to preserve edges during the process

$$\min_{u\in BV(\Omega)}\frac{\lambda}{2}\|Au-f\|^2+TV(u). \quad (8)$$

It has proved to be quite efficient for regularizing images without smoothing the boundaries of the objects.

This problem was first analyzed on strong L^p topology by Acar and Vogel [1]. We define a subspace as

$$BV_0(\Omega)=\left\{u\in BV(\Omega)\,\middle|\,\int_\Omega u dx=0\right\}.$$

Here, let $\mathbf{1}$ be a constant function whose result is always equal to 1, and A is required to meet $A\mathbf{1}\neq 0$ and $\langle Av,A\mathbf{1}\rangle=0,\forall v\in BV_0$, respectively.

Then, let us describe some notations used throughout the total variation theory and assume the size or image to be

$m \times n$. We denotes that $\mathbf{X} \subseteq \mathbb{R}^{m\times n}$ and $\mathbf{Y} = \mathbf{X} \times \mathbf{X}$. Inner products in the spaces X and Y are defined as

$$(u, v) = \sum_{i=1}^{m}\sum_{j=1}^{n} u_{i,j}v_{i,j} \text{ and } \left\langle \widehat{\mathbf{g}}, \widehat{\mathbf{h}} \right\rangle = \sum_{i=1}^{m}\sum_{j=1}^{n}\sum_{s=1}^{2} \widehat{\mathbf{g}}^2_{i,j,s}\widehat{\mathbf{h}}^2_{i,j,s},$$

for $u, v \in \mathbf{X}$ and $\widehat{\mathbf{g}} := (g_1, g_2) \in \mathbf{Y}$, $\widehat{\mathbf{h}} := (h_1, h_2) \in \mathbf{Y}$. Furthermore, we define the related norm as

$$\|u\|_2 := \sqrt{\sum_{i=1}^{m}\sum_{j=1}^{n} u^2_{i,j}} \text{ and } \|\widehat{\mathbf{g}}\|_{2,1} := \sum_{i=1}^{m}\sum_{j=1}^{n}\sqrt{\sum_{s=1}^{2} \widehat{\mathbf{g}}^2_{i,j,s}}.$$

In addition, we set the discrete gradient $\nabla u_{i,j} = (\nabla^+_x u_{i,j}, \nabla^+_y u_{i,j})$, where $\nabla^+_x u_{i,j}$ and $\nabla^+_y u_{i,j}$ denote the difference operators as

$$\nabla^+_x u_{i,j} = \begin{cases} u_{i+1,j} - u_{i,j} & \text{if } 1 \le i < m \\ u_{1,j} - u_{i,j} & \text{if } i = m, \end{cases}$$

$$\nabla^+_y u_{i,j} = \begin{cases} u_{\imath,j+1} - u_{i,j} & \text{if } 1 \le j < n \\ u_{i,1} - u_{i,j} & \text{if } j = n. \end{cases}$$

Formally, the corresponding backward difference operators can be defined by

$$\nabla^-_x u_{i,j} = \begin{cases} u_{i,j} - u_{i-1,j} & \text{if } 1 < i \le m \\ u_{i,j} - u_{m,j} & \text{if } i = 1, \end{cases}$$

$$\nabla^-_y u_{i,j} = \begin{cases} u_{i,j} - u_{i,j-1} & \text{if } 1 < j \le n \\ u_{i,j} - u_{i,n} & \text{if } j = 1. \end{cases}$$

In the case of a discrete setting, the divergence theorem can be described as

$$-\mathrm{div}\boldsymbol{\rho} \cdot u = \boldsymbol{\rho} \cdot \nabla u$$

for $u \in \mathbf{X}$ and $\boldsymbol{\rho} = \left(\rho^1, \rho^2\right) \in \mathbf{Y}$, where $-\mathrm{div}$ denotes the adjoint operator of ∇. Then we have

$$\mathrm{div}\boldsymbol{\rho}_{i,j} \quad = \quad \nabla^-_x \rho^1_{i,j} + \nabla^-_y \rho^2_{i,j}.$$

In model (8), the regularization term and the fidelity term should have a weight parameter λ, which is difficult to determine even with σ known. Therefore, a constraint model is used to construct without parameters here.

$$\begin{aligned} &\min_u TV(u) \\ &s.t. D_f(u) \leqslant c(\sigma), \end{aligned} \tag{9}$$

where f is noisy image, D_f is a distance function, and $c(\sigma)$ is a function with respect to the noise level σ. Thus, the key issue is how to define the set C, or how to choose the distance function D_f and the function $c(\sigma)$. For MRI, because the noise is mainly Rician, after taking into account the similarity between Gaussian noise and Rician noise, ℓ^2 norm is used here. The Rician noise is similar to Gaussian noise with a higher signal-to-noise ratio(SNR), but the result would be too smooth if we use this definition to deal with a MRI with a lower SNR. We could use a smaller $c(\sigma)$ by $c(\sigma) = \sqrt{M} \times k \times \sigma$, $k \in [0, 1]$.

Then, a characteristic function can be used to replace the constraint condition,

$$\delta_C(u) = \begin{cases} 0, & if \quad u \in C \\ +\infty, & otherwise \end{cases}, C = \{u | D_f(u) \leqslant c(\sigma)\}. \tag{10}$$

So, the model can be rewritten as

$$\min_u TV(u) + \delta_C(u). \tag{11}$$

B. Primal dual method

This image processing could be viewed as an inverse problem modeled as

$$\min_x g(x) + f(Kx), \tag{12}$$

where $g(x)$ is the data fidelity term that ensures that the solution will not too far from the input data, $f(Kx)$ is the regularization term describing the characteristic of a clean image, and K is a linear operator.

Based on the definition of the Legendre-Fenchel transformation

$$f^*(x) = \sup_y \langle x, y\rangle - f(y),$$

and for a proper convex function f, we get the description

$$f = f^{**}.$$

If we replace the original function with a quadratic dual method, the original minimization problem becomes a saddle point problem

$$\min_x \max_y \langle Kx, y\rangle + g(x) - f^*(y), \tag{13}$$

which the first order optimal condition is

$$\begin{cases} Kx \in \partial f^*(y) \\ -K^*y \in \partial g(x), \end{cases} \tag{14}$$

where K^* is the adjoint conjugate of K, which is more general.

Using a proximal point algorithm, the problem's solution is [3]

$$\begin{cases} y^{n+1} = \arg\min_y f^*(y) - \langle K\overline{x}^n, y\rangle + \frac{1}{2\alpha}||y - y^n||^2 \\ x^{n+1} = \arg\min_x \langle Kx, y^{n+1}\rangle + g(x) + \frac{1}{2\beta}||x - x^n||^2 \\ \overline{x}^{n+1} = x^{n+1} + \theta\left(x^{n+1} - x^n\right). \end{cases} \tag{15}$$

We rewrite the problem and get

$$\begin{cases} y^{n+1} = (I + \alpha\partial f^*)^{-1}\left(y^n + \alpha K\overline{x}^n\right) \\ \qquad = prox_{\alpha,f^*}\left(y^n + \alpha K x^n\right) \\ x^{n+1} = (I + \beta\partial g)^{-1}\left(x^n - \beta K^* y^{n+1}\right) \\ \qquad = prox_{\beta,g}\left(x^n - \beta K^* y^{n+1}\right) \\ \overline{x}^{n+1} = x^{n+1} + \theta\left(x^{n+1} - x^n\right), \end{cases} \tag{16}$$

where $\alpha > 0$ and $\beta > 0$ are step sizes of the primal and dual variables, respectively. How to solve this saddle problem, where I is the identity operator and ∂ denotes the subgradient defined by $\partial\hbar(\bar{y}) := \{v | \hbar(\bar{\chi}) - \hbar(y) \geq (v, \bar{\chi} - \bar{y})\}$ at the point $\bar{y}$ for a function $\hbar$. Then the convergence result of the scheme (16) would be given as follows.

Theorem 4.1: Assume that the min-max problem (13) has a saddle point (x^*, y^*) and let $\alpha\beta\|K\|^2 < 1$, then the sequence (x^n, y^n) generated by the strategy (16) converges to (x^*, y^*) by choosing some suitable original values$(x^0, y^0) \in X\times$ Y and $\bar{x} = x^0$.

To establish the theorem (4.1), we can refer to Theorem 1 presented by Chambolle and Pock [3]. Notably, the PDM eliminates the need for matrix inversion when the functions $g(x)$ and $f^*(y)$ are separable in terms of the variables x and y. Consequently, this method is well-suited for tackling large-scale problems in machine learning and medical image processing [7], [27].

C. The proposed model based on the PDM

Based on the primal dual method, we rewrite this model

$$TV(u) = \|\nabla u\|_1 = \sum_i \sum_j \sqrt{(\nabla_x u_{i,j})^2 + (\nabla_y u_{i,j})^2}.$$

Let $f(x) = \|x\|_1$, then $TV(u) = f(\nabla u)$, and

$$\begin{aligned} f^*(y) &= \sup_x \langle x, y\rangle - f(x) \\ &= \sup_x \langle x, y\rangle - \|x\|_1 \\ &= \begin{cases} 0, & y_i \in [-1, 1] \\ +\infty, & otherwise \end{cases} \\ &= \delta_D(y), \end{aligned}$$

where δ_D is a characteristic function of set $D = \{p | \|p\|_\infty \leqslant 1\}$. Therefore, going back to Eqn 11, we can get

$$TV(u) = \sup_p \langle u, -divp\rangle - \delta_D(p),$$

and the model can be rewritten as

$$\min_u \sup_p \langle u, -divp\rangle - \delta_D(p) + \delta_C(u). \tag{17}$$

So, the algorithm for the model solution can be an iteration of two projections[3]:

$$\begin{cases} p^{n+1} = P_D\left(p^n + \alpha \nabla \overline{u}^n\right) \\ u^{n+1} = P_C\left(u^n + \beta divp^{n+1}\right) \\ \overline{u}^{n+1} = u^{n+1} + \theta\left(u^{n+1} - u^n\right). \end{cases} \tag{18}$$

The first projection can be solved using the procedure.

$$p_{i,j}^{n+1} = \frac{p_{i,j}^n + \alpha \nabla \overline{u}_{i,j}^n}{max\left(1, \left|p_{i,j}^n + \alpha \nabla \overline{u}_{i,j}^n\right|\right)}, \tag{19}$$

where

$$\nabla \overline{u}_{i,j}^n = \left(\nabla_x \overline{u}_{i,j}^n, \nabla_y \overline{u}_{i,j}^n\right), p_{i,j}^n = \left(p_{x\,i,j}^n, p_{y\,i,j}^n\right),$$

and

$$\left|p_{i,j}^n + \alpha \nabla \overline{u}_{i,j}^n\right| = \sqrt{\left(p_{x\,i,j}^n + \alpha \nabla_x \overline{u}_{i,j}^n\right)^2 + \left(p_{y\,i,j}^n + \alpha \nabla_y \overline{u}_{i,j}^n\right)^2}.$$

However, since Rician is a noise dependent on signal, both its variance and expectation are determined by the true signal value. To get a desired result, k must be changed according to different pixel values. We can standardize the noise, and the constraint condition is changed to

$$\left\| \frac{E(u,\sigma) - f}{\sqrt{\mathrm{var}(u,\sigma)}} \right\|_2^2 \leqslant M, \tag{20}$$

where $E(u,\sigma)$ is the expectation, and $\mathrm{var}(u,\sigma)$ is the variance of the Rician noise. Both the expectation and variance can be calculated by the probability density function

$$\begin{cases} E(u,\sigma) = \sigma\sqrt{\frac{\pi}{2}} \exp(-\frac{u^2}{4\sigma^2}) U^* \\ \mathrm{var}\,(u,\sigma) = 2\sigma^2 + u^2 - (E(u,\sigma))^2, \end{cases}$$

where

$$U^* = \left[\left(1 + \frac{u^2}{2\sigma^2}\right) I_0\left(\frac{u^2}{4\sigma^2}\right) + \frac{u^2}{2\sigma^2} I_1\left(\frac{u^2}{4\sigma^2}\right)\right].$$

But with the constraint condition, $C = \left\{u \middle| \left\| \frac{E(u,\sigma)-f}{\sqrt{\mathrm{var}(u,\sigma)}} \right\|_2^2 \leqslant M \right\}$, the first projection to C will be difficult to calculate. Thus, the model is modified as

$$\left\{ \begin{array}{c} \min_u TV(u) \\ s.t. \left\| \frac{u-f}{\sqrt{\mathrm{var}(E^{-1}(u,\sigma),\sigma)}} \right\|_2^2 \leqslant M \end{array} \right\}. \tag{21}$$

Here $E^{-1}(u,\sigma)$ denotes $E(u,\sigma) \to u$, and u_0 is the solution. Then, $E^{-1}(u_0,\sigma)$ will be a better restoration for Rician noise image. Let $\mathrm{var}(u,\sigma) = c^2(\frac{u}{\sigma})\sigma^2$, and we get

$$\begin{aligned} &\min_u TV(u) \\ &s.t. \left\| \frac{u-f}{c\left(\frac{E^{-1}(u,\sigma)}{\sigma}\right)} \right\|_2^2 \leqslant M\sigma^2, \end{aligned} \tag{22}$$

where

$$\begin{aligned} c^2\left(\frac{u}{\sigma}\right) &= \frac{\mathrm{var}\,(u,\sigma)}{\sigma^2} \\ &= 2 + \left(\frac{u}{\sigma}\right)^2 - \frac{\pi}{2}\exp\left(-\left(\frac{u^2}{2\sigma^2}\right)\right)(U^*)^2. \end{aligned} \tag{23}$$

Since $E^{-1}(u_0,\sigma)$ is not easy to solve, on the one side, at higher SNR, the deviation caused by Rician noise is not obvious. On the other side, at a lower SNR, the original signal is basically overwhelmed by noise and difficult to recover. Therefore, a approximate function could be used as

$$E_{i,j}^{-1}(u,\sigma) \approx \begin{cases} 0, & \frac{u_{i,j}}{\sigma} \leqslant 2 \\ u_{i,j}, & otherwise. \end{cases} \tag{24}$$

Then, we get the set $C = \left\{u \middle| \left\| \frac{u-f}{c\left(\frac{E^{-1}(u,\sigma)}{\sigma}\right)} \right\|_2^2 \leqslant M\sigma^2 \right\}$.

The second projection is still not easy to solve, but we can give an approximate solution as follows,

$$u^{n+1} = f + \frac{u^n + \beta divp^{n+1} - f}{max\left(1, \left\| \frac{(u^n + \beta divp^{n+1})}{c(E^{-1}(u^n)/\sigma)} \right\| / \left(\sqrt{M}\sigma\right)\right)}. \tag{25}$$

Based on formulas (23) and (24), we get the result

$$\begin{cases} c\left(\frac{E^{-1}(u,\sigma)}{\sigma}\right) = c(0), & \frac{u}{\sigma} \leqslant 2 \\ c\left(\frac{E^{-1}(u,\sigma)}{\sigma}\right) \approx 1, & otherwise. \end{cases} \tag{26}$$

Assuming c is an approximate constant, we get

$$P_C(x) = \arg\min_u \|u - x\|_2^2 + \gamma\left(\|(u-f)/c\|^2 - M\sigma^2\right).$$

If $\gamma = 0$, then $\|(u-f)/c\|^2 \leqslant M\sigma^2$, which means $u = x$ when $\|(x-f)/c\|^2 \leqslant M\sigma^2$.

If $\gamma \neq 0$, by the Euler-Lagrange equation, we get

$$u_{i,j} = \frac{x_{i,j}c_{i,j}^2 + \gamma f_{i,j}}{c_{i,j}^2 + \gamma},$$

and

$$\left\| \frac{u-f}{c} \right\|^2 = M\sigma^2.$$

Therefore,

$$\gamma = \frac{\|c\,(x-f)\,\|}{\sqrt{M}\sigma} - c^2$$

and formula (25) can be obtained. While the solution is surely not the optimal one, this approximation ensure the solution is in the set C and not far from initial point x.

V. Number Results

In this section, some number experiments will be shown to illustrate the effectiveness of our proposed approach about Rician noise level estimation and its image restoration capability. We know that in natural images, the gradient matrix of image information is generally sparse. To better compare the experiments, we prepare one natural image in original images.

A total of four images were chosen for testing, as depicted in Figure 1. These include one natural image titled "Cameraman" with a resolution of 256×256 pixels, and three MR images "Brain"(512×512), "Body"(648×648), "Leg"(880×880). To quantitatively assess the quality of the restoration results, two commonly used evaluation metrics in image processing were employed: the Peak Signal-to-Noise Ratio (PSNR) and the Structural Similarity Index (SSIM). All experiments were conducted on a desktop computer equipped with an Intel Core i7 3.30 GHz processor, 8.0 GB of RAM, running Windows 10 (64-bit) and the MATLAB (R2019a) operating environment. The algorithm terminated either when the maximum number of iterations reached 500 or when a specified relative error threshold is met.

(a) (b) (c) (d)

Fig. 1: Original images, (a)"Cameraman", (b)"Brain", (c)"Body"and (d)"Leg" are used in the numerical implementations.

In the first experiment, we estimate the Rician noise level. As discussed in section 3, if the patch size is too small, the smooth regions cannot be estimated accurately. On the contrary, if the patch size is too large, a large number of patches contain boundary information. Therefore, the patch size is set at 13, and we estimate the noise level for the chosen images under different Rician noise intensities. We test a comparison based on the natural image and the MRI. Obviously, the image "Cameraman" includes many approximated cartoon regions and the image "Brain" has the cerebellum, thalamus, and many nerve tissues. Figure 2 shows the estimation results in relation to different noise levels. "Cameraman" exerts a large interference on the noise estimation due to the complex texture area, such as a large area of grass when the noise intensity is low. The image "Brain" does not have too many areas with complex texture, so it has a good performance in noise intensity estimation.

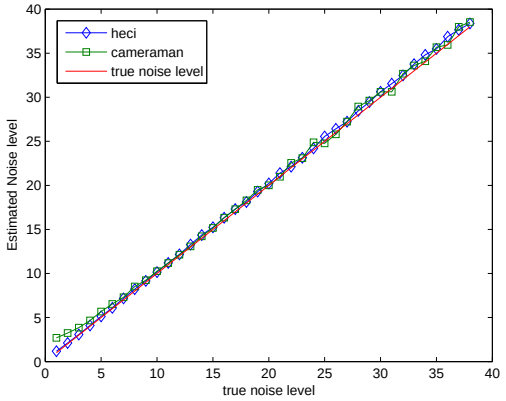

Fig. 2: Rician noise estimation of image "Cameraman" and "Brain"

In the second experiment, we use the results of the new noise intensity estimation method for MRI restoration. In order to quantitatively compare the performance, we list the restored results with the values of PSNR and SSIM. The related data for the restored images are shown in Table I. It is obvious that the estimated results appear to be very competitive.

In the denoising case, the test images are degraded by Rician noise with standard deviation $\sigma = 10, 20, 30$, respectively. Figure 3 shows the degraded images and the restoration effect with different noise levels for four original images. Specifically, Figure 4 shows the zoomed-in parts of denoising results of different Rician noise levels, where the corresponding regions are marked green, for instance, one region includes various organs, the spine, lungs, and muscle tissue in the image "Body". It can be seen from the figures that our proposed method has played a good role in image restoration. Because the Rician noise is signal related, and the deviation caused by noise covers the changes of the original image details, in the restored image, some details of the original image are erased. Thus, it is difficult to find or distinguish these details on a noisy image. Figure 5 shows the visual comparison of colorbar to the difference in clean images and restored images. The results of colorbar of zoomed-in parts in Figure 4 with $\sigma = 5, 10, 15$. As can be seen, the colorbar shows a more efficient restoration if the color is more shaded.

VI. Conclusion

In this paper, we propose a new method for estimating Rician noise levels and a parameter-free MRI restoration model. Given the high resolution of MRI, we employ a patch-based method to achieve a more accurate estimation of the Rician noise level, simplifying the estimation process. Using the estimated noise intensity, we construct a new distance generalization function, which allows us to establish a suitable constraint. As a result, an image restoration model without parameters is established. According to the primal dual algorithm, the model can be solved successfully. Various

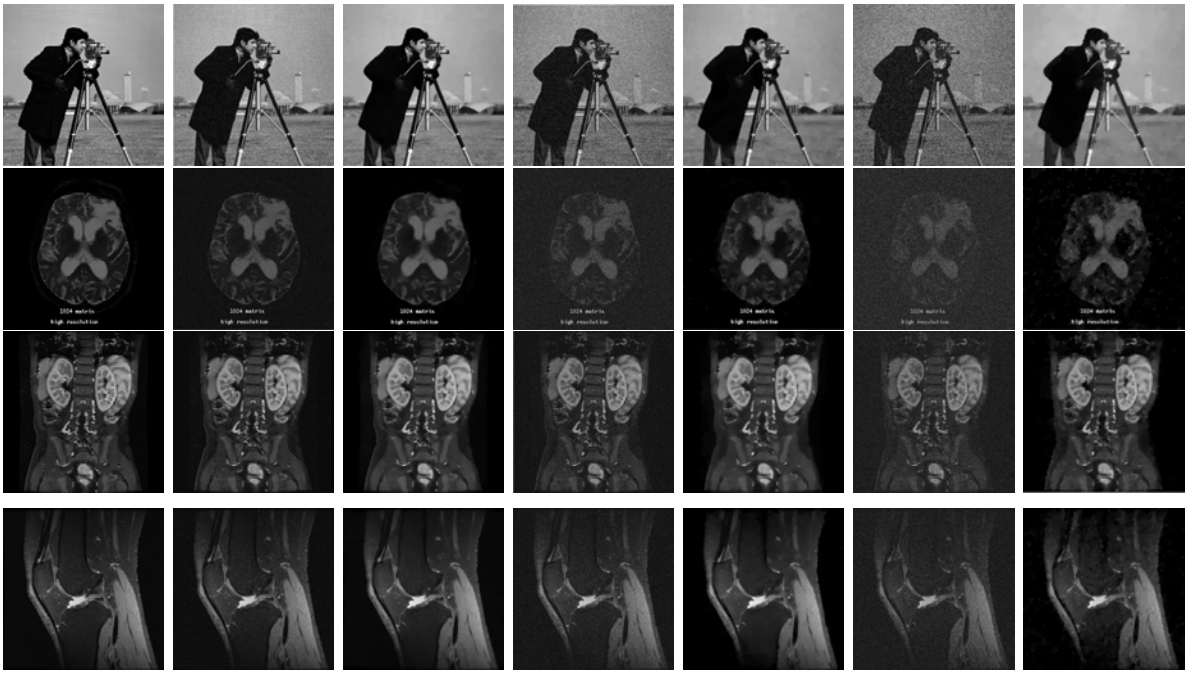

(a) (b) (c) (d) (e) (f) (g)

Fig. 3: The restoration results with different noise levels $\sigma = 10, 20, 30$ under Rician Noise. Column (a) is the original images. Column (b) is the noisy images and column (c) is the restored images with $\sigma = 10$. Column (d) is the noisy images and column (e) is the restored images with $\sigma = 20$. Column (f) is the noisy images and column (g) is the restored images with $\sigma = 30$.

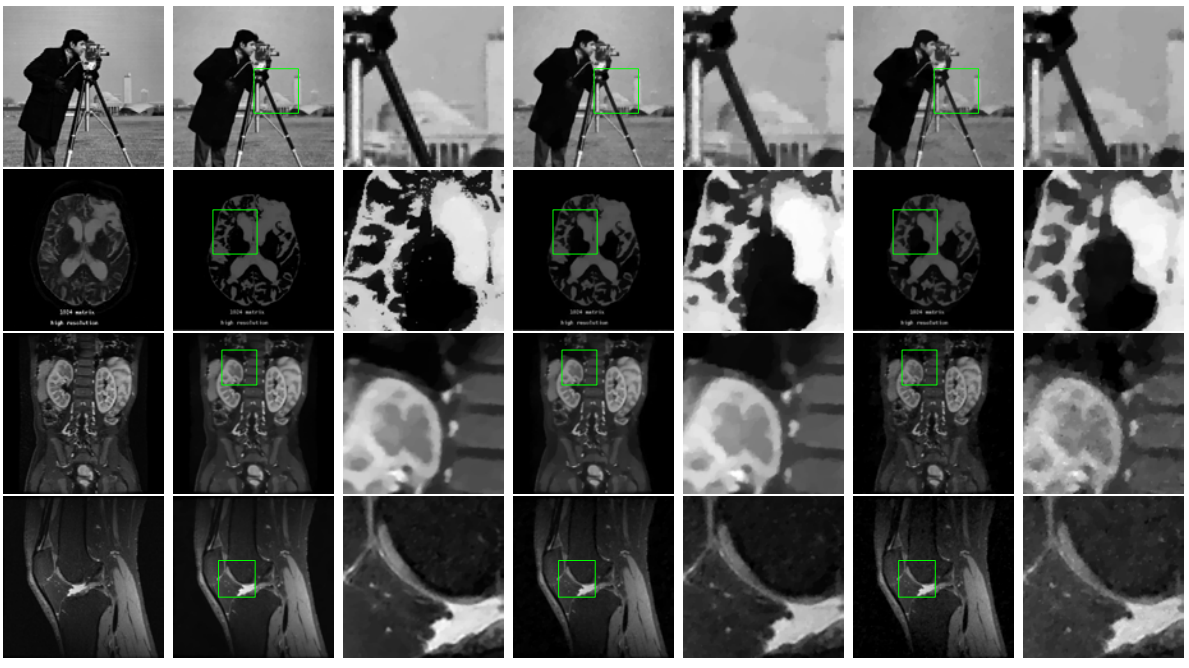

(a) (b) (c) (d) (e) (f) (g)

Fig. 4: Zoomed- in parts of denoising results are shown by different noise levels under Rician Noise, where the corresponding regions are marked green. Column (a) is the original images. Column (c) is the zoomed-in parts of denoising results of column (b) with $\sigma = 10$. Column (e) is the zoomed-in parts of denoising results of column (d) with $\sigma = 20$. Column (g) is the zoomed-in parts of denoising results of column (f) with $\sigma = 30$.

TABLE I: The results of PSNR and SSIM with different Rician noise levels in Fig. 1 (a)-(d).

Noise	σ =5		σ=10		σ=15		σ=20		σ=30	
Image	Fig. 1 (a)									
	PSNR	SSIM	PSNR	SSIM	PSNR	SSIM	PSNR	SSIM	PSNR	SSIM
Noisy Image	34.2511	0.8472	28.3321	0.6438	25.7996	0.5339	22.2555	0.4031	18.7732	0.2846
Restored Image	35.4223	0.9405	32.2075	0.9029	30.8251	0.8686	28.2340	0.8267	25.3841	0.7275
Image	Fig. 1 (b)									
	PSNR	SSIM	PSNR	SSIM	PSNR	SSIM	PSNR	SSIM	PSNR	SSIM
Noisy Image	34.7019	0.5204	29.2683	0.3776	27.1828	0.3665	24.0314	0.2276	21.0009	0.1395
Restored Image	41.4413	0.9700	39.3607	0.9466	37.7227	0.9451	35.3378	0.8671	32.5878	0.8345
Image	Fig. 1 (c)									
	PSNR	SSIM	PSNR	SSIM	PSNR	SSIM	PSNR	SSIM	PSNR	SSIM
Noisy Image	33.9251	0.8495	28.1916	0.7795	25.9019	0.7015	22.5966	0.6444	19.5133	0.5267
Restored Image	38.9691	0.9803	35.3406	0.9513	33.9418	0.9328	31.9653	0.8503	30.4385	0.8195
Image	Fig. 1 (d)									
	PSNR	SSIM	PSNR	SSIM	PSNR	SSIM	PSNR	SSIM	PSNR	SSIM
Noisy Image	33.9251	0.8495	28.7039	0.8985	26.7396	0.8481	23.1775	0.6929	20.0438	0.5145
Restored Image	38.9691	0.9803	37.1185	0.9477	35.9581	0.9071	32.5873	0.7626	30.4256	0.6337

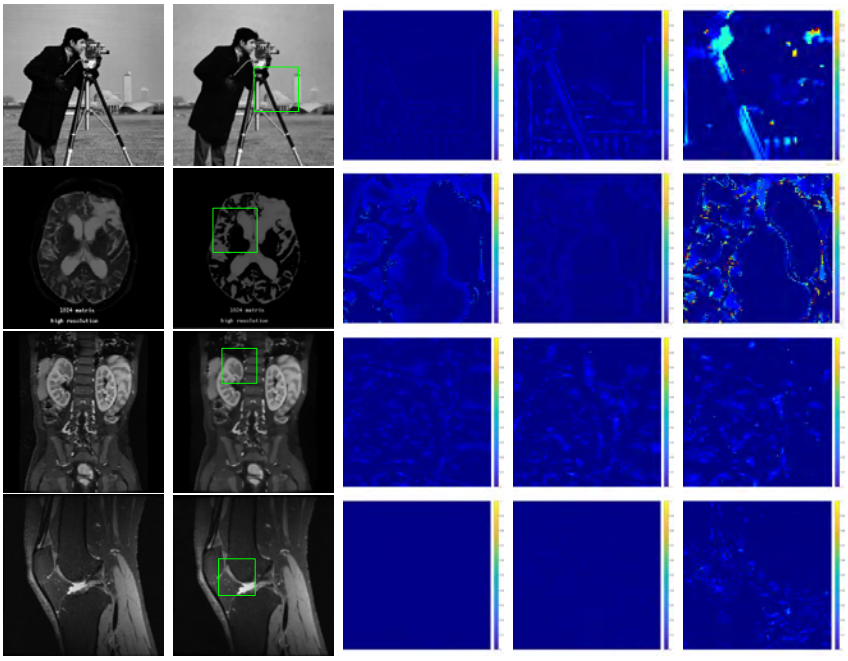

(a) (b) (c) (d) (e)

Fig. 5: Visual comparison of colorbar to the difference between the clean images in Column (a) and restored images in Column (b). Column (c)-(e) are the results of colorbar of zoomed-in parts in column (b) with $\sigma = 5, 10, 15$. The colorbar shows a more efficient restoration if the color is more shaded.

numerical experiments demonstrate that good recovery results can be achieved by solving the model with the estimated Rician noise intensity.

REFERENCES

[1] R. Acar, C. Vogel, "Analysis of Total Variation Penalty Methods for Ill-Posed Problems," *IOP Publishing Ltd*, pp. 1217-1229, 1994.

[2] B. Billot, C. Magdamo, Y. Cheng, et al, "Robust machine learning segmentation for large-scale analysis of heterogeneous clinical brain MRI datasets," *Proceedings of the National Academy of Sciences*, vol. 120, no. 9: e2216399120, 2023.

[3] A. Chambolle, T. Pock, "A first-order primal-dual algorithm for convex problems with applications to imaging," *Journal of Mathematical Imaging and Vision*, vol. 40, no. 1, pp. 120-145, 2011.

[4] A. Chaudhari, J. Kulkarni, "Noise estimation in single coil MR images," *Biomedical Engineering Advances*, vol. 2, pp. 1-9, 2021.

[5] L. Chen, T. Zeng, "A convex variational model for restoring blurred images with large Rician noise," *Journal of Mathematical Imaging and Vision*, vol. 53, no. 3, pp. 1598-1625, 2014.

[6] H. Cheng, "Variation of noise in multi-run functional MRI using generalized autocalibrating partially parallel acquisition (GRAPPA)," *Journal of Magnetic Resonance Imaging*, vol. 35, no. 2, pp. 462-470, 2012.

[7] E. Chouzenoux, A. Contreras, J. Pesquet, et al, "Convergence Results for Primal-Dual Algorithms in the Presence of Adjoint Mismatch," *SIAM Journal on Imaging Sciences*, vol. 16, no. 1, pp. 1-34, 2023.

[8] C. Constantinides, E. Atalar, E. McVeigh, "Signal-to-noise measurements in magnitude images from NMR phased arrays," *Magnetic Resonance in Medicine*, vol. 38, pp. 852-857, 1997.

[9] P. Coupé, J. Manjón, E. Gedamu, et al, "Robust Rician noise estimation for MR images" *Medical Image Analysis*, vol. 14, no. 4, pp. 483-493, 2010.

[10] S. Esedoglu, S. Osher, "Decomposition of images by the anisotropic Rudin-Osher-Fatemi model," *Communications on Pure and Applied Mathematics*, vol. 57, no. 12, pp. 1609-1626, 2004.

[11] A. Foi, "Noise estimation and removal in MR imaging: the variance-stabilization approach," *IEEE International Symposium on Biomedical Imaging: From Nano to Macro*, pp. 1809-1814, 2011.

[12] Z. Gao, Y. Guo, J. Zhang, et al, "Hierarchical Perception Adversarial Learning Framework for Compressed Sensing MRI," *IEEE Transactions on Medical Imaging*, pp. 1558-254X, 2023.

[13] J. Guo, Y. Zhang, "Improved Particle Swarm Optimization with Mean-based Prediction," *IAENG International Journal of Computer Science*, vol. 51, no. 2, pp. 162-168, 2024.
[14] R. Henkelman, "Measurement of signal intensities in the presence of noise in MR images," *Medical Physics*, vol. 12, no. 2, pp. 232-233, 1985.
[15] N. Idalisa, M. Rivaie, N. Fadhilah, et al, "An Improved Version of Rivaie-Mohd-Ismail-Leong Conjugate Gradient Method With Application in Image Restoration," *IAENG International Journal of Applied Mathematics*, vol. 53, no. 3, pp. 1051-1060, 2023.
[16] L. Li, X. Qiu, M. Jing, et al, "Block Compressed Sensing Image Reconstruction via Untrained Network Priors," *IAENG International Journal of Computer Science*, vol. 50, no. 2, pp. 505-511, 2023.
[17] R. Nowak, "Wavelet-based Rician noise removal for magnetic resonance imaging," *IEEE Transactions on Image Processing*, vol. 8, no. 10, pp. 1408-1419, 1999.
[18] A. Papoulis, "Probability, Random Variables and Stochastic Processes," *Tata McGraw-Hill*, pp. 25-66, 2002.
[19] M. Pizzolato, E. Canales-Rodríguez, et al, "Axial and radial axonal diffusivities and radii from single encoding strongly diffusion-weighted MRI," *Medical Image Analysis*, vol. 86:102767, 2023.
[20] B. Shi, F. Gu, Z. Pang, et al, "Remove the salt and pepper noise based on the high order total variation and the nuclear norm regularization," *Applied Mathematics and Computation*, vol. 421: 126925, 2022.
[21] D. Shin, R. Park, S. Yang, et al, "Block-based noise estimation using adaptive Gaussian filtering," *IEEE Transactions on Consumer Electronics*, vol. 51, no. 1, pp. 218-226, 2005.
[22] J. Sijbers, A. Dekker, "Maximum likelihood estimation of signal amplitude and noise variance from MR data," *Magnetic Resonance in Medicine*, vol. 51, no. 3, pp. 586-594, 2004.
[23] J. Sijbers, D. Poot, A. Dekker, et al, "Automatic estimation of the noise variance from the histogram of a magnetic resonance image," *Physics in Medicine and Biology*, vol. 52, no. 5, pp. 1335-1348, 2007.
[24] A. Stefano, P. White, W. Collis, "Training methods for image noise level estimation on wavelet components," *Eurasip Journal on Applied Signal Processing*, vol. 16, pp. 2400-2407, 2004.
[25] Y. Wang, Z. Pang, Y. Duan, et al, "Image retinex based on the non-convex TV-type regularization," *Inverse Problems & Imaging*, vol. 15, no. 6, pp. 1381, 2021.
[26] Y. Chen, W. Lai, W. He, et al, "Hyperspectral Compressive Snapshot Reconstruction via Coupled Low-Rank Subspace Representation and Self-Supervised Deep Network," *IEEE Transactions on Image Processing*, vol. 33, pp. 926-941, 2024.
[27] Y. Zhang, L. Xiao, "Stochastic primal-dual coordinate method for regularized empirical risk minimization," *Journal of Machine Learning Research*, no. 18, pp. 1-42 2017.